J. Fluid Mech. (1975), *vol.* 69, *part* 2, *pp.* 209–227
Printed in Great Britain

Steady flow in rapidly rotating variable-area rectangular ducts

By JOHN S. WALKER

Department of Theoretical and Applied Mechanics, University of Illinois, Urbana

(Received 14 August 1974)

Steady liquid flow in a variable-area rectangular duct rotating rapidly about an axis perpendicular to its centre-line is treated. This problem is significant because the idea of driving a liquid through a rotating system has been largely overlooked by rotating-fluid dynamicists and because it closely resembles the flow inside the impellers of centrifugal pumps and hydraulic turbines. For a prototype formed by joining a semi-infinite constant-area duct and a semi-infinite duct with straight diverging walls, the flow in the diverging duct is carried entirely by large, $O(E^{-\frac{1}{3}})$ velocities in a boundary layer of thickness $O(E^{\frac{1}{3}})$ adjacent to one of the (side) walls parallel to the axis of rotation, where E is the (small) Ekman number. With a vertical axis of rotation this high-velocity boundary layer is adjacent to the side wall on the right when facing in the flow direction. For a diverging or converging duct placed between two semi-infinite constant-area ducts, large, $O(E^{-\frac{1}{3}})$ velocities occur in side-wall boundary layers on both sides of the variable-area duct and on the left and right sides of the upstream and downstream constant-area ducts respectively. The existence of high-velocity side layers in rapidly rotating rectangular ducts should be relatively easy to prove experimentally and actual measurements of their velocity profiles would provide a good test of the present theory.

1. Introduction

This paper treats steady incompressible flow in rectangular ducts with plane parallel sides at $z = \pm 1$ and symmetrically diverging or converging top and bottom at $y = \pm f(x)$, where the co-ordinates are rotating about an axis parallel to the y axis with respect to some inertial frame. The constant speed of rotation is assumed to be sufficiently large for inertial effects to be neglected throughout and for viscous effects to be confined to thin boundary layers and free shear layers.

The general form of the solution for $f' \neq 0$ is derived in §2. The $O(1)$ flow in the inviscid core follows the geostrophic surfaces $x =$ constant and the $O(1)$ flow in the x direction is carried by large, $O(E^{-\frac{1}{3}})$ velocities in boundary layers of thickness $O(E^{\frac{1}{3}})$ adjacent to the sides, where E is the (small) Ekman number. The three-dimensional boundary-value problem governing the flow in each of these side layers is reduced to a two-dimensional equation. Since these two equations involve x derivatives f must be given for all x in order to solve the problem for any x.

A prototype formed by joining two semi-infinite ducts with straight walls with

$f' = 0$ for $x < 0$ and $f' =$ constant $= s > 0$ for $x > 0$ is considered in §3. The two-dimensional equations governing the $E^{\frac{1}{3}}$ side layers downstream ($x > 0$) are reduced to eigenvalue problems involving infinite-dimension square matrices. Eigenfunction expansions are used to represent the solutions in these layers with the coefficients in these expansions determined by matching with the solution in the upstream duct ($x < 0$).

Approximate solutions to the eigenvalue problems are given in §4. The numerical results reveal that $O(E^{-\frac{1}{3}})$ velocities occur only in the $E^{\frac{1}{3}}$ side layer at $z = 1$ in the downstream duct. The asymptotic form of the flow in this layer for $x \to \infty$ is presented for several values of s. The structures of the free shear layers at $x = 0$ in this prototype are discussed in §5.

Extension of the analysis for the prototype with straight walls to more general duct geometries is considered in §6. Application of the analysis of §§2–4 to a general diverging or converging duct placed between two constant-area ducts ($f' = 0$ for $x < 0$ and $x > l$) reveals that $O(E^{-\frac{1}{3}})$ velocities occur in both $E^{\frac{1}{3}}$ side layers in the diverging duct ($0 < x < l$), in the $E^{\frac{1}{3}}$ side layer at $z = -1$ in the upstream duct ($x < 0$) and in the $E^{\frac{1}{3}}$ side layer at $z = 1$ in the downstream duct ($x > l$). The high-velocity side layers in the constant-area ducts carry no net flow but provide a redistribution of the flow in the y direction, which is necessary in order to match the flows in the $E^{\frac{1}{3}}$ side layers in the diverging duct. Barcilon (1967) has also considered flow through a rotating system and discussed vertical transport in the $E^{\frac{1}{3}}$-layer with $E^{-\frac{1}{3}}$ velocities. Extensions to ducts with symmetrically diverging or converging sides and to ducts with non-rectangular cross-sections are also discussed in §6.

2. Formulation for a general duct

The flow considered here is incompressible and steady relative to a Cartesian co-ordinate system rotating at a constant angular velocity $\boldsymbol{\omega} = \omega\hat{\mathbf{y}}$ with respect to some inertial system, so that the non-dimensional governing equations are

$$\nabla . \mathbf{v} = 0, \quad Ro(\mathbf{v} . \nabla)\mathbf{v} = -\nabla\Phi - \hat{\mathbf{y}} \times \mathbf{v} + E\nabla^2\mathbf{v}, \tag{1a, b}$$

where

$$\Phi = (p/\rho + \phi - \tfrac{1}{2}\omega^2 a^2)/2\omega U_c d$$

is the reduced pressure (Greenspan 1968, p. 6). Here $\hat{\mathbf{y}}$ is a unit vector in the y direction, $\mathbf{v}$ is the velocity, $Ro = U_c/2\omega d$ and $E = \nu/2\omega d^2$ are the Rossby and Ekman numbers respectively, p is the true pressure, ρ is the density, ϕ is the gravitational potential, a is the perpendicular distance from the axis of rotation, U_c is a characteristic velocity, d is a characteristic length and ν is the (constant) kinematic viscosity.

The flow is confined by a rectangular duct with its centre-line perpendicular to the axis of rotation, with plane parallel sides (parallel to the axis of rotation) and with symmetrically diverging or converging top and bottom (see figure 1). Half the distance between the sides is used for d and the average velocity at some cross-section, say $x = 0$, is used for U_c, so that

$$\int_{-1}^{1} \int_{-f(0)}^{f(0)} u(0, y, z)\, dy\, dz = 4f(0). \tag{2}$$

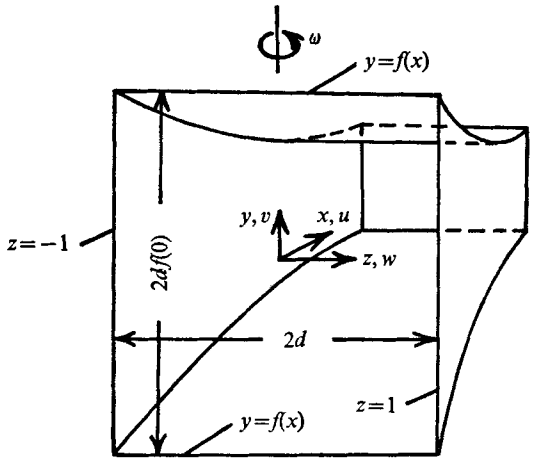

FIGURE 1. Duct.

The boundary conditions are

$$\mathbf{v} = 0 \quad \text{at} \quad y = \pm f(x), \quad z = \pm 1. \tag{3a,b}$$

Together with the governing equations (1) these form a homogeneous problem whose solution is normalized by the condition (2).

For a sufficiently large ω

$$Ro \ll 1, \quad E \ll 1, \tag{4a,b}$$

so that the inertial and viscous terms in (1 *b*) can be neglected outside boundary layers and free shear layers. It turns out that the present solution involves large, $O(E^{-\frac{1}{3}})$ velocities in boundary layers of thickness $O(E^{\frac{1}{3}})$ adjacent to the sides, so that the condition $Ro \ll E^{\frac{2}{3}}$ is required in order that the inertial terms may be neglected everywhere (Walker 1974). Under condition (4 *b*) the flow region can be divided into several parts, certain viscous terms in (1 *b*) being negligible in each subregion. The various subregions (shown in figure 2) are (*a*) the core, (*a'*) primary Ekman layers, (*b*), (*c*) side layers at $z = \mp 1$ respectively, (*b'*), (*c'*) secondary Ekman layers and (*b''*), (*c''*) corner regions.

The variables in the primary Ekman layers are determined locally by the tangential velocity outside and automatically match the core variables provided that the latter satisfy the usual Ekman conditions at $y = \pm f$, which relate the normal velocity to the normal component of the relative vorticity (measured in the rotating reference frame). A similar result holds for the secondary Ekman layers, so that they can also be ignored as long as the side-layer variables satisfy certain modified Ekman conditions at $y = \pm f$. Each corner region is needed to represent properly a singularity in the side-layer solution there. In the corner regions there is very little simplification in (1) beyond neglect of the inertial terms and these regions have never been fully analysed. Fortunately the first approximation can be obtained everywhere else without considering the corner regions in detail.

Expansions in E may be used to determine the flow in each region. First the co-ordinates within a region are rescaled such that all derivatives are $O(1)$. The

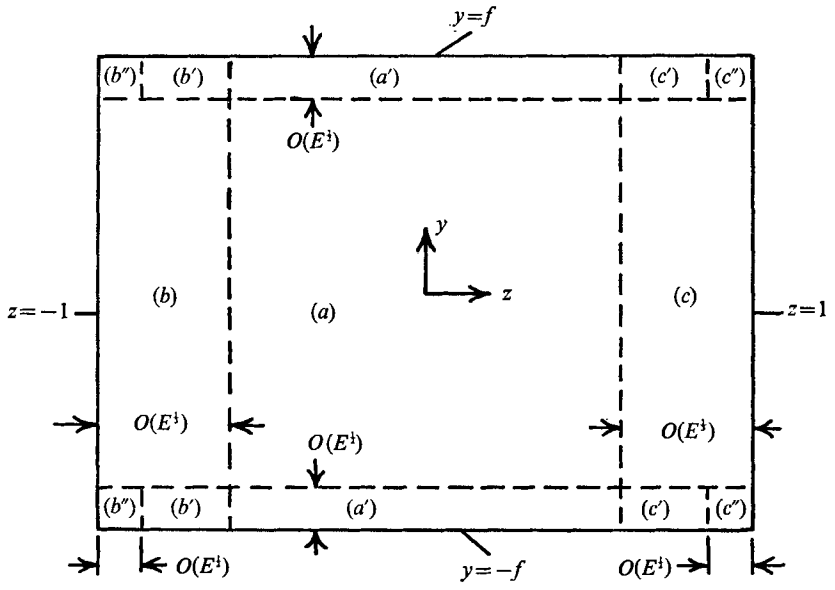

FIGURE 2. x section showing flow subregions for a general duct.

variables $\mathbf{v}$ and Φ are then written as series in ascending fractional powers of E with coefficients which are functions of the (possibly scaled) co-ordinates alone. These asymptotic expansions are not simply power series in some fractional power of E; the appropriate power of E for each term depends upon the previous terms and upon the expansions in adjacent regions which must be matched. Some series begin with negative powers of E. Ultimately the justification for the powers used in each expansion lies in the compatibility of the complete solution. The coefficients are denoted by $\mathbf{v}_p^r$ and Φ_p^r, where the superscript r denotes the region and the subscript p denotes the power of E for this term.

The leading terms in the core expansions satisfy (1) (with inertial and viscous terms neglected and with no rescaling) and the Ekman conditions

$$f'u_0^a \mp v_0^a = 0 \quad \text{at} \quad y = \pm f,$$

and thus have the form

$$u_0^a = v_0^a = 0, \quad w_0^a = -d\psi/dx, \quad \Phi_0^a = \psi,$$

where $\psi(x)$ is an integration function. The $O(1)$ core flow is geostrophic, the duct's cross-sections $x =$ constant being the geostrophic surfaces, so there is no $O(1)$ flow along the duct within the core.

Since condition (2) requires a total flow of $4f(0)$ along the duct and since the order of magnitude of the velocity in an Ekman layer is the same as that of the tangential velocity outside, u must be $O(E^{-\frac{1}{3}})$ in at least one of the side layers. There is thus a dramatic difference between flow in a duct with diverging or converging top and bottom as here and flow in a duct with parallel top and bottom, in which the total flow is carried by an $O(1)$ core velocity u (see § 3). The z co-ordinate within each side layer is stretched by introducing new co-ordinates

$$\zeta = E^{-\frac{1}{3}}(z \mp 1)$$

for the layers at $z = \pm 1$ respectively. After some manipulation (1) become

$$\partial v^r_{-\frac{1}{3}}/\partial y + \partial^3 u^r_{-\frac{1}{3}}/\partial \zeta^3 = 0, \tag{5a}$$

$$\partial u^r_{-\frac{1}{3}}/\partial y - \partial^3 v^r_{-\frac{1}{3}}/\partial \zeta^3 = 0, \tag{5b}$$

$$\partial \Phi^r_0/\partial \zeta = u^r_{-\frac{1}{3}}, \quad w^r_0 = \partial^2 u^r_{-\frac{1}{3}}/\partial \zeta^2 - \partial \Phi^r_0/\partial x, \tag{5c,d}$$

where $r = b$ or c. The appropriate Ekman conditions are once again simply

$$f' u^r_{-\frac{1}{3}} \mp v^r_{-\frac{1}{3}} = 0 \quad \text{at} \quad y = \pm f. \tag{6}$$

The boundary conditions (3b) become

$$u^r_{-\frac{1}{3}} = v^r_{-\frac{1}{3}} = w^r_0 = 0 \quad \text{at} \quad \zeta = 0, \tag{7a–c}$$

while matching with the core solution yields

$$u^b_{-\frac{1}{3}} = v^b_{-\frac{1}{3}} = 0, \quad \Phi^b_0 = \psi \quad \text{as} \quad \zeta \to \infty \tag{8a–c}$$

and

$$u^c_{-\frac{1}{3}} = v^c_{-\frac{1}{3}} = 0, \quad \Phi^c_0 = \psi \quad \text{as} \quad \zeta \to -\infty. \tag{9a–c}$$

Henceforth only diverging ducts will be considered. Solutions for converging ducts are obtained by simply changing the signs of certain variables in the solutions for geometrically similar diverging ducts (i.e. the solution for a duct with $f' > 0$ is normalized to give a total flow of $-4f(0)$).

Following Howard (1969), separation of variables is used to solve (5a, b). For the layer at $z = -1$, the solution which satisfies conditions (6), (7a, b) and (8a, b) is

$$u^b_{-\frac{1}{3}} = \sum_{n=1}^{\infty} d_n(x)\, F_n(\zeta) \cos[(n-\alpha)\pi y f^{-1}], \tag{10a}$$

$$v^b_{-\frac{1}{3}} = -\sum_{n=1}^{\infty} d_n(x)\, F_n(\zeta) \sin[(n-\alpha)\pi y f^{-1}], \tag{10b}$$

where

$$F_n = \nu_n \sin(3^{\frac{1}{2}} \nu_n \zeta) \exp(-\nu_n \zeta), \quad \nu_n = \tfrac{1}{2}[(n-\alpha)\pi f^{-1}]^{\frac{1}{3}},$$
$$\alpha = \pi^{-1} \arctan f',$$

and for the layer at $z = 1$, the solution which satisfies conditions (6), (7a, b) and (9a, b) is

$$u^c_{-\frac{1}{3}} = \sum_{n=0}^{\infty} b_n(x)\, G_n(\zeta) \cos[(n+\alpha)\pi y f^{-1}], \tag{11a}$$

$$v^c_{-\frac{1}{3}} = \sum_{n=0}^{\infty} b_n(x)\, G_n(\zeta) \sin[(n+\alpha)\pi y f^{-1}], \tag{11b}$$

where

$$G = \mu_n \sin(3^{\frac{1}{2}} \mu_n \zeta) \exp(\mu_n \zeta), \quad \mu_n = \tfrac{1}{2}[(n+\alpha)\pi f^{-1}]^{\frac{1}{3}}.$$

The trick in these separation-of-variables solutions is to replace $u^r_{-\frac{1}{3}}$ and $v^r_{-\frac{1}{3}}$ with

$$\hat{U} = u^r_{-\frac{1}{3}} \cos(\alpha\pi y f^{-1}) + v^r_{-\frac{1}{3}} \sin(\alpha\pi y f^{-1}),$$
$$\hat{V} = v^r_{-\frac{1}{3}} \cos(\alpha\pi y f^{-1}) - u^r_{-\frac{1}{3}} \sin(\alpha\pi y f^{-1})$$

so that the boundary conditions (6) become simply

$$\hat{V} = 0 \quad \text{at} \quad y = \pm f$$

(Howard 1969). The solution (10a) is introduced into (5c) to obtain Φ^b_0, the integration function being determined by condition (8c), while the solution (11a),

equation (5c) and condition (9c) give Φ_0^c. Finally, w_0^b and w_0^c are given by (5d). The fact that the solutions (10) begin with $n = 1$ while the solutions (11) begin with $n = 0$ results in a fundamental difference between the two side layers. It turns out that this difference is reflected in the fact that there can be a flow in the layer at $z = 1$ while there is no flow in the core or in the layer at $z = -1$, but that a flow cannot exist in the layer at $z = -1$ without an accompanying flow in both the core and the layer at $z = 1$.

Side layers of thickness $O(E^{\frac{1}{4}})$ occur in some rotating rectangular ducts. However, the velocity along such a layer is independent of y so these layers can only occur when the distance between the top and bottom does not change along the layer. Thus $E^{\frac{1}{4}}$-layers do not occur in the present duct as long as $f' \neq 0$.

Only the determination of the functions $\psi(x)$, $b_n(x)$ and $d_n(x)$ remains. The only condition (7c) which has not yet been applied yields a pair of equations governing these functions, the independent variables being x and y. Since these equations contain x derivatives, $f(x)$ must be given for all x (or suitable boundary conditions added at the ends of a finite interval) in order to determine the solution for any x. If $f'' \neq 0$ the equations can only be solved using numerical relaxation schemes, while for the special case $f'' = 0$ the equations can be reduced to a pair of eigenvalue problems. Fortunately this special case represents a prototype and the solution for it can be used to approximate solutions for more general ducts.

3. Prototype with straight walls

A prototype is formed by joining two semi-infinite ducts with straight walls, one with diverging top and bottom and one with parallel top and bottom, so that

$$f = \begin{cases} c & \text{for} \quad x < 0, \\ c + sx & \text{for} \quad x > 0, \end{cases}$$

where c and s are positive constants. The flow subregions in a y section (i.e. x, z plane) of this duct are shown in figure 3 together with the letters used as superscripts for the coefficients in the expansions for each region. There are also Ekman layers of thickness $O(E^{\frac{1}{2}})$ above and below each of these regions as well as corner regions with $O(E^{\frac{1}{2}})$ by $O(E^{\frac{1}{2}})$ cross-sections along the corners at $y = \pm f$, $z = \pm 1$ and at $x = 0$, $y = \pm c$.

Downstream duct $x > 0$

The analysis of §2 applies in the downstream duct ($x > 0$) and the superscripts a, b and c denote the same regions as there. Application of the boundary condition (7c) to the w_0^b and w_0^c derived from solutions (10a) and (11a) now gives

$$4f\psi' = 3^{\frac{1}{2}} \sum_{n=1}^{\infty} \{[fd_n' - (n-\alpha)\pi d_n] \cos[(n-\alpha)\pi y f^{-1}] + d_n(n-\alpha)\pi s y f^{-1} \sin[(n-\alpha)\pi y f^{-1}]\}, \qquad (12a)$$

$$4f\psi' = 3^{\frac{1}{2}} \sum_{n=0}^{\infty} \{[fb_n' + (n+\alpha)\pi b_n] \cos[(n+\alpha)\pi y f^{-1}] + b_n(n+\alpha)\pi s y f^{-1} \sin[(n+\alpha)\pi y f^{-1}]\}, \qquad (12b)$$

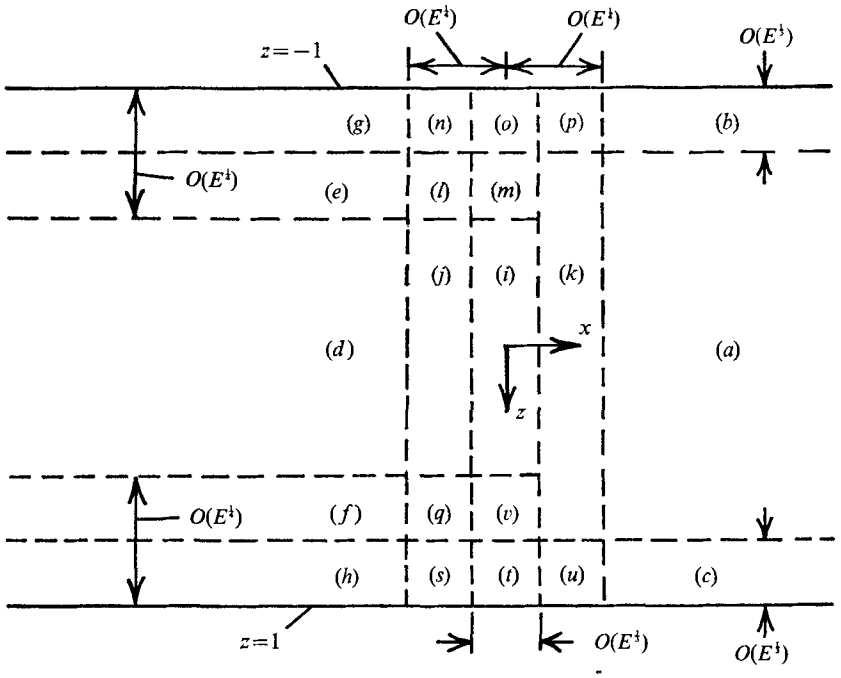

FIGURE 3. y section showing flow subregions for a prototype with straight walls.

where $f = c + sx$, $\alpha = \pi^{-1}\arctan s$ and a prime denotes differentiation with respect to x.

Equations (12) can be converted into two infinite sets of simultaneous ordinary differential equations by multiplying each by $\cos(k\pi y f^{-1})$ and integrating with respect to y from $-f$ to f:

$$\sum_{n=1}^{\infty}(-1)^n\{fd_n'[(n-\alpha+k)^{-1}+(n-\alpha-k)^{-1}] + sd_n(n-\alpha)[(n-\alpha+k)^{-2}+(n-\alpha-k)^{-2}]\} = -H_k, \tag{13a}$$

$$\sum_{n=0}^{\infty}(-1)^n\{fb_n'[(n+\alpha+k)^{-1}+(n+\alpha-k)^{-1}] + sb_n(n+\alpha)[(n+\alpha+k)^{-2}+(n+\alpha-k)^{-2}]\} = H_k, \tag{13b}$$

where
$$H_k = \begin{cases} 8\pi f\psi'/3^{\frac{1}{2}}\sin(\alpha\pi) & \text{for } k = 0, \\ 0 & \text{for } k = 1, 2, 3, \ldots. \end{cases}$$

The next step is to reduce (13) to a pair of decoupled eigenvalue problems involving infinite-dimension square matrices. First the substitutions

$$b_n = B_n f^{\lambda}, \quad \psi = d_n = 0$$

lead to an eigenvalue problem

$$\lambda\mathbf{B} = \mathbf{M}\mathbf{B},$$

where $\mathbf{B}$ is a vector with components B_n ($n = 0, 1, 2, 3, \ldots$) and $\mathbf{M}$ is a square matrix defined by

$$\mathbf{M} = \mathbf{L}^{-1}\mathbf{K},$$

with
$$L_{kn} = (n+\alpha+k)^{-1} + (n+\alpha-k)^{-1},$$
$$K_{kn} = -(n+\alpha)[(n+\alpha+k)^{-2} + (n+\alpha-k)^{-2}]$$

for $k, n = 0, 1, 2, \ldots$. There is an infinite number of discrete eigenvalues λ_i with an eigenvector $\mathbf{B}^{(i)} = \{B_n^{(i)}\}$ for each eigenvalue. Next the substitutions

$$b_n = B_n f^\gamma, \quad \psi = \Psi f^\gamma, \quad d_n = D_n f^\gamma$$

lead to a second eigenvalue problem

$$\gamma \mathbf{D} = \mathbf{N}\mathbf{D},$$

where $\mathbf{D}$ is a vector with components D_n $(n = 1, 2, 3, \ldots)$ and $\mathbf{N}$ is a square matrix defined by

$$\mathbf{N} = \mathbf{P}^{-1}\mathbf{R},$$

with
$$P_{kn} = (n-\alpha+k)^{-1} + (n-\alpha-k)^{-1},$$
$$R_{kn} = -(n-\alpha)[(n-\alpha+k)^{-2} + (n-\alpha-k)^{-2}]$$

for $k, n = 1, 2, 3, \ldots$. Again there is an infinite number of discrete eigenvalues γ_i with an eigenvector $\mathbf{D}^{(i)} = \{D_n^{(i)}\}$ for each eigenvalue. The values of $\Psi^{(i)}$ and $B_n^{(i)}$ $(n = 0, 1, 2, \ldots)$ for each eigenvalue are obtained from (13 *a*) with $k = 0$ and (13 *b*) respectively. The only eigenvalue which is missed by this scheme is $\lambda_0 = 0$, for which $B_n^{(0)} = D_n^{(0)} = 0$, corresponding to an arbitrary additive constant pressure $\Psi^{(0)}$. For the first set of eigenvalues there is flow in the side layer at $z = 1$ alone. Flow in the side layer at $z = -1$ cannot exist without a non-zero value of ψ'. Thus for the second set of eigenvalues there is a pressure gradient in the core which is balanced by the Coriolis force produced by an $O(1)$ transverse core velocity w_0^a. This core velocity means that there is an $O(1)$ flow into or out of the side layer at $z = 1$ at each cross-section, so there must also be a flow in this layer. Together, the two sets of eigenfunctions are complete. These eigenvalue problems will be treated numerically in § 4.

The solution (10 *a*) can be integrated over the cross-section of the side layer at $z = -1$ to obtain the total flow through this layer,

$$Q^b = -\tfrac{1}{2} \times 3^{\frac{1}{2}} f \pi^{-1} \sin(\alpha\pi) \sum_{n=1}^{\infty} (-1)^n d_n (n-\alpha)^{-1}, \tag{14a}$$

and similarly integrating solution (11 *a*) gives

$$Q^c = -\tfrac{1}{2} \times 3^{\frac{1}{2}} f \pi^{-1} \sin(\alpha\pi) \sum_{n=0}^{\infty} (-1)^n b_n (n+\alpha)^{-1} \tag{14b}$$

for the layer at $z = 1$. Therefore values of λ_i and γ_i greater than minus one must be excluded because the corresponding flows are unbounded as $x \to \infty$, the one exception being $\gamma_0 = 0$, which corresponds to zero flow everywhere. The solution in the downstream duct can now be expanded in the solutions corresponding to the remaining eigenvalues. The coefficients in this expansion are determined by matching the side-layer variables with the variables in the intersection regions (p) and (u) respectively.

Matching at $x = 0$ and upstream duct $x < 0$

In the intersection regions (n), (o), (p), (s), (t) and (u) the x velocity u is at most $O(E^{-\frac{1}{3}})$, so that the x component of (1 b), together with the boundary condition

$$w = 0 \quad \text{at} \quad \zeta = 0,$$

in all of these regions, yields the matching conditions

$$\Phi_0^b(0, y, 0) = \Phi_0^g(0, y, 0), \quad \Phi_0^c(0, y, 0) = \Phi_0^h(0, y, 0), \tag{15a, b}$$

where the independent variables in the upstream $E^{\frac{1}{3}}$ side layers (g) and (h) are also x, y and ζ. The independent variables in the upstream $E^{\frac{1}{4}}$ side layers (e) and (f) are x, y and ξ, where

$$\xi = E^{-\frac{1}{4}}(z \mp 1) \tag{16}$$

for the layers at $z = \pm 1$ respectively.

The core solution for fully developed flow in a constant-area rectangular duct is

$$u_0^d = 1, \quad v_0^d = w_0^d = 0, \quad \Phi_0^d = z,$$

where an inessential additive constant in Φ_0^d has been dropped. Since fully developed flow is symmetric in z, only the side layers (e) and (g) at $z = -1$ are considered. The variables in the $E^{\frac{1}{4}}$ side layer (e) for fully developed flow are

$$\Phi_0^e = -1, \quad \Phi_{\frac{1}{4}}^e = \xi + 2^{\frac{1}{4}}c^{\frac{1}{2}} \exp(-\xi 2^{-\frac{1}{4}}c^{-\frac{1}{2}}),$$
$$u_0^e = \partial\Phi_{\frac{1}{4}}^e/\partial\xi, \quad v_0^e = w_0^e = w_{\frac{1}{4}}^e = 0, \quad v_{\frac{1}{4}}^e = -y\,\partial^4\Phi_{\frac{1}{4}}^e/\partial\xi^4.$$

In the $E^{\frac{1}{3}}$ side layer (g), which matches the non-zero value of this $v_{\frac{1}{4}}^e$ at $\xi = 0$,

$$u_{\frac{1}{4}}^g = 2^{-\frac{3}{4}}c^{-\frac{3}{2}}6^{-1}\zeta^3 + \sum_{n=1}^{\infty} [\hat{a}_n \exp(-2\sigma_n\zeta) - \hat{b}_n \exp(-\sigma_n\zeta)$$
$$\times \cos(3^{\frac{1}{2}}\sigma_n\zeta) - \hat{c}_n \exp(-\sigma_n\zeta)\sin(3^{\frac{1}{2}}\sigma_n\zeta)]\cos(n\pi yc^{-1}),$$

$$v_{\frac{1}{4}}^g = -2^{-\frac{3}{4}}c^{-\frac{3}{2}}y + \sum_{n=1}^{\infty} [\hat{a}_n \exp(-2\sigma_n\zeta) + \hat{b}_n \exp(-\sigma_n\zeta)$$
$$\times \cos(3^{\frac{1}{2}}\sigma_n\zeta) + \hat{c}_n \exp(-\sigma_n\zeta)\sin(3^{\frac{1}{2}}\sigma_n\zeta)]\sin(n\pi yc^{-1}),$$

where
$$\sigma_n = 2^{-1}(n\pi c^{-1})^{\frac{1}{3}}, \quad \hat{a}_n = \hat{b}_n = -2^{-\frac{3}{4}}c^{-\frac{1}{2}}(-1)^n n^{-1}\pi^{-1},$$
$$\hat{c}_n = -3^{\frac{1}{2}}\hat{a}_n, \quad \partial\Phi_{\frac{1}{12}}^g/\partial\zeta = u_{\frac{1}{4}}^g, \quad \Phi_0^g = -1.$$

If the flow in the upstream duct ($x < 0$) remained fully developed until it entered the upstream $E^{\frac{1}{4}}$ free shear layer (j) and intersection regions (l), (n), (q) and (s), then

$$\Phi_0^g(0, y, 0) = -1, \quad \Phi_0^h(0, y, 0) = 1.$$

Equations (15) could then be reduced to two infinite sets of linearly independent simultaneous equations involving the unknown coefficients in the eigenfunction expansion of the downstream solution by multiplying by $\cos(k\pi yc^{-1})$ and integrating between $y = \pm c$. However, since some of the eigenvalues λ_i and γ_i are excluded these two sets of equations would represent an overdetermined system. Thus matching places certain restrictions on $\Phi_0^g(0, y, 0)$ and $\Phi_0^h(0, y, 0)$ and the

flow must deviate from fully developed flow upstream of $x = 0$ in order to satisfy these restrictions. In particular, since

$$\psi(0) - \Phi_0^b(0, y, 0) = \int_0^\infty u^b_{-\frac{1}{3}}(0, y, \zeta)\, d\zeta,$$

$$\Phi_0^c(0, y, 0) - \psi(0) = \int_{-\infty}^0 u^c_{-\frac{1}{3}}(0, y, \zeta)\, d\zeta$$

represent the vertical distributions of the flows entering the downstream side layers at $z = \mp 1$ from the intersection regions (p) and (u), and since the exclusion of certain eigenvalues appears to mean that these distributions cannot be independent of y, it follows that the upstream flow must involve vertical redistribution of the flow. It will turn out that the prototype is a special case in which these distributions happen to be independent of y but that this is not true of more general ducts.

The first-order horizontal velocity in the upstream core (d) and in the $E^{\frac{1}{4}}$ layers (e), (f), (j) and (k) is independent of y (Taylor–Proudman theorem). The vertical distribution of flow in the $E^{\frac{1}{3}}$ free shear layer (i) must also be independent of y since

$$\int_{-\infty}^\infty w^i_{-\frac{1}{3}}\, d\eta = \Phi_0^j(0, z) - \Phi_0^k(0, z),$$

where $\Phi_0^{j,k}$ are functions of (X, z) and

$$X = E^{-\frac{1}{4}}x, \quad \eta = E^{-\frac{1}{3}}x. \tag{17a,b}$$

In fact $\Phi_0^j(0, z) = \Phi_0^k(0, z)$ and this $E^{\frac{1}{3}}$ layer carries no $O(1)$ flow (see §5). The velocity in the intersection regions (l), (m), (n), (o), (p), (q), (s), (t), (u) and (v) is too small to account for an $O(1)$ vertical flow. Therefore the upstream $E^{\frac{1}{3}}$ side layers (g) and (h) must accomplish the required vertical flow redistribution.

The variables in the upstream $E^{\frac{1}{3}}$ side layers satisfy equations (5) and boundary conditions (7) with $r = g$ or h as well as the conditions

$$v^r_{-\frac{1}{3}} = 0 \quad \text{at} \quad y = \pm c, \tag{18}$$

$$u^g_{-\frac{1}{3}} = v^g_{-\frac{1}{3}} = 0, \quad \Phi_0^g = \Phi_0^e(x, 0) \quad \text{as} \quad \zeta \to \infty, \tag{19a–c}$$

$$u^h_{-\frac{1}{3}} = v^h_{-\frac{1}{3}} = 0, \quad \Phi_0^h = \Phi_0^f(x, 0) \quad \text{as} \quad \zeta \to -\infty, \tag{20a–c}$$

where $\Phi_0^{e,f}$ are functions of (x, ξ) and ξ is given by (16). Once again separation of variables gives the solutions of $(5a, b)$ satisfying conditions $(7a, b)$ and (18) and, for the layer at $z = -1$, conditions $(19a, b)$, so that

$$u^g_{-\frac{1}{3}} = -\sum_{n=1}^\infty a_n(x) \exp(-\sigma_n \zeta) \sin(3^{\frac{1}{2}}\sigma_n \zeta) \cos(n\pi y c^{-1}), \tag{21a}$$

$$v^g_{-\frac{1}{3}} = \sum_{n=1}^\infty a_n(x) \exp(-\sigma_n \zeta) \sin(3^{\frac{1}{2}}\sigma_n \zeta) \sin(n\pi y c^{-1}), \tag{21b}$$

or, for the layer at $z = 1$, conditions $(20a, b)$, so that

$$u^h_{-\frac{1}{3}} = \sum_{n=1}^\infty c_n(x) \exp(\sigma_n \zeta) \sin(3^{\frac{1}{2}}\sigma_n \zeta) \cos(n\pi y c^{-1}), \tag{22a}$$

$$v^h_{-\frac{1}{3}} = \sum_{n=1}^\infty c_n(x) \exp(\sigma_n \zeta) \sin(3^{\frac{1}{2}}\sigma_n \zeta) \sin(n\pi y c^{-1}), \tag{22b}$$

where

$$\sigma_n = \tfrac{1}{2}(n\pi c^{-1})^{\frac{1}{3}}.$$

From (21*a*) and (22*a*)

$$\int_{-c}^{c} u^r_{-\frac{1}{3}}\, dy = 0.$$

Thus there is no net flow along one of these side layers, so that if the flow is in the $+x$ direction near the plane of symmetry $y = 0$ then it must be in $-x$ direction near the top and bottom. These layers receive flow from the intersection regions (*n*) and (*s*), redistribute it vertically and return it to the same regions (*n*) and (*s*).

The determination of the functions a_n and c_n remains. Equation (5*c*), together with solutions (21*a*) and (22*a*) and conditions (19*c*) and (20*c*), gives Φ^r_0 and then (5*d*) gives w^r_0. The only remaining condition (7*c*) now gives

$$\partial\Phi^e_0(x,0)/\partial x = \partial\Phi^f_0(x,0)/\partial x = 0, \tag{23a,b}$$

$$a'_n - n\pi c^{-1}a_n = c'_n + n\pi c^{-1}c_n = 0. \tag{23c,d}$$

The flow must become fully developed as $x \to -\infty$, so that the appropriate solutions of (23) are

$$\Phi^e_0(x,0) = -1, \quad \Phi^f_0(x,0) = 1, \quad a_n = A_n \exp(n\pi c^{-1}x), \quad c_n = 0.$$

Thus there can be a high-velocity sheet jet adjacent to the side $z = -1$, but there cannot be one adjacent to the side $z = 1$. This sheet jet at $z = -1$ has as much reverse flow as forward flow and thus accomplishes a vertical flow redistribution while carrying no net flow itself. The coefficients A_n are determined by the matching (15*a*) while $\Phi^h_0(0,y,0) = 1$ in (15*b*) (see §4).

There is no net flow in the $E^{\frac{1}{3}}$ side layers because the $n = 0$ term is missing from the series (21*a*) and (22*a*). As Howard (1969) points out, the $n = 0$ term in the series (11*a*) degenerates into an $E^{\frac{1}{4}}$ side layer as $\alpha \to 0$, so it is reasonable to expect that the $E^{\frac{1}{4}}$ side layers (*e*) and (*f*) might involve $O(E^{-\frac{1}{4}})$ velocities and might thus carry an $O(1)$ flow. Solutions for such layers exist and match the core variables as $\xi \to \pm\infty$ for the layers at $z = \mp 1$ respectively, but involve non-zero values of $u^{e,f}_{-\frac{1}{4}}$ at $\xi = 0$, which the $E^{\frac{1}{3}}$ side layers (*g*) and (*h*) cannot match and also satisfy the boundary conditions (3*b*). Thus $E^{\frac{1}{4}}$ side layers involving $O(E^{-\frac{1}{4}})$ velocities do not occur.

The $O(E^{-\frac{1}{3}})$ velocities in the $E^{\frac{1}{3}}$ side layer (*g*) do not create any $O(1)$ perturbations in the core (*d*) or in the $E^{\frac{1}{4}}$ side layers (*e*) and (*f*). The upstream core variables are given by

$$u^d_0 = \partial\Phi^d_0/\partial z, \quad v^d_0 = 0, \quad w^d_0 = -\partial\Phi^d_0/\partial x,$$

where $\Phi^d_0(x,z)$ satisfies

$$\partial^2\Phi^d_0/\partial x^2 + \partial^2\Phi^d_0/\partial z^2 = 0. \tag{24}$$

Equation (24) follows from the $O(E^{\frac{1}{2}})$ Ekman conditions

$$v^d_{\frac{1}{2}} = \mp 2^{-\frac{1}{2}}(\partial^2\Phi^d_0/\partial x^2 + \partial^2\Phi^d_0/\partial z^2) \quad \text{at} \quad y = \pm c$$

together with the fact that Φ^d_0 and $v^d_{\frac{1}{2}}$ are independent of y. The boundary conditions on Φ^d_0 are

$$\Phi^d_0 = z \quad \text{as} \quad x \to -\infty, \qquad \Phi^d_0 = \pm 1 \quad \text{at} \quad z = \pm 1$$

and the values of Φ_0^d at $x = 0$ are given by matching variables in the core (d) and the upstream $E^{\frac{1}{4}}$ free shear layer (j). Once $\Phi_0^d(0, z)$ is known the solution of (24) can be obtained using separation of variables or a numerical relaxation scheme, for example. No specific solutions for Φ_0^d are presented here.

To first order the solutions in the $E^{\frac{1}{4}}$ side layers (e) and (f) are given by the solutions for fully developed flow (which match $u_0^d = 1$) multiplied by $u_0^d(x, \pm 1)$ at each x section. The structure of the $E^{\frac{1}{3}}$ side layers (g) and (h) matching these layers is also given by a simple rescaling of the fully developed flow structure, where this is superimposed upon the high-velocity structure for the layer (g) at $z = -1$.

The upstream and downstream $E^{\frac{1}{3}}$ side layers will be considered further in §4 and the free shear layers (i), (j) and (k) will be discussed in §5.

4. Eigenvalues and the asymptotic flow for $x \to \infty$

The eigenvalue problems derived in §3 can be solved approximately by truncating the infinite-dimension matrices **L**, **K**, **P** and **R** after $k, n = N$. A standard computer program for finding the eigenvalues of a general (asymmetric) real square matrix then yields $N+1$ values for λ_i and N values for γ_i. In each case this approximate scheme gives both real and complex eigenvalues, the magnitude of the real part of each complex eigenvalue being greater than the magnitudes of all the real eigenvalues. For $N = 70$ there are 46, 28, 13 and 0 real values for both λ_i and γ_i for $\alpha = 0{\cdot}125$, $0{\cdot}25$, $0{\cdot}375$ and $0{\cdot}5$ respectively. Testing with $N = 80$ and 90 reveals that all but two of the real values for $N = 70$ and any α are independent of N to eight significant figures and are thus eigenvalues for the original problems, which correspond to $N \to \infty$.

For the real eigenvalues which do not change when N is increased, several patterns emerge from the numerical analysis. First,

$$\lambda_0 = -1, \quad \lambda_i < -1, \quad \gamma_i > 0 \quad \text{for all} \quad i \neq 0.$$

Thus all γ_i except $\gamma_0 = 0$ are excluded and no λ_i is excluded. The solutions in the side layer (b) at $z = -1$ and in the core (a) are

$$u^b_{-\frac{1}{3}} = v^b_{-\frac{1}{3}} = 0, \quad \Phi_0^b = \Psi'(0), \quad \psi = \Psi'(0).$$

The matching (15a) gives

$$\Psi'(0) = -1, \quad A_n = 0 \quad \text{for} \quad n = 1, 2, 3, \ldots.$$

For this prototype $O(E^{-\frac{1}{3}})$ velocities do not occur in either the upstream $E^{\frac{1}{3}}$ side layers (g) and (h) or the downstream $E^{\frac{1}{3}}$ side layer (b) at $z = -1$ and $O(1)$ velocities do not occur in the downstream core (a). This is not true of most other duct geometries (see §6).

The second pattern emerging from the numerical analysis is the equation

$$\lambda_i = -1 - \gamma_i \tag{25}$$

for $i = 0, 1, 2, 3, \ldots$, where the eigenvalues λ_i and γ_i are arranged in ascending magnitude. Finally, the differences between adjacent eigenvalues (either λ_i or γ_i)

$\alpha = 0{\cdot}125$	$\alpha = 0{\cdot}25$	$\alpha = 0{\cdot}375$
0·0000	0·0000	0·0000
7·6463	3·7741	2·5571
15·6312	7·7565	5·2118
23·6278	11·7528	7·8763
31·6266	15·7516	10·5423
39·6260	19·7510	13·2087
47·6256	23·7506	15·8752
55·6254	27·7504	18·5418
63·6252	31·7502	21·2084
71·6250	35·7500	23·8750
79·6248	39·7498	26·5416
87·6246	43·7487	29·2082

TABLE 1. First twelve eigenvalues γ_i for $\alpha = 0{\cdot}125$, 0·25 and 0·375. $\lambda_i = -\gamma_i - 1$

quickly approach asymptotic values as i increases, these values being 8, 4 and $2\frac{2}{3}$ for $\alpha = 0{\cdot}125$, 0·25 and 0·375 respectively. Note that these asymptotic values are α^{-1}. The first dozen γ_i are given in table 1 for $\alpha = 0{\cdot}125$, 0·25 and 0·375, while the first dozen λ_i follow from (25).

The coefficients in the eigenfunction expansion of the solution for the downstream $E^{\frac{1}{3}}$ side layer at $z = 1$ are now determined for a given α by the matching (15*b*) with $\Phi_0^h(0, y, 0) = 1$. These coefficients are not presented here. The basic characteristics of the flow in this side layer are revealed by the asymptotic form of the flow for $x \to \infty$, so only velocity profiles for this asymptotic flow and not those for various x sections are presented here.

Equation (13*b*) with $k = 0$, $b_n = B_n f^{\lambda}$ and $\psi = 0$ becomes

$$(\lambda + 1) \sum_{n=0}^{\infty} (-1)^n B_n (n + \alpha)^{-1} = 0,$$

so that either $\lambda = -1$ or, according to (14*b*), $Q^c = 0$. Therefore the flow associated with $\lambda_0 = -1$ carries the entire flow of 4*c*. The flows associated with λ_i for $i = 1, 2, 3, \ldots$, involve no net flow and are needed in order for the side layer (*c*) to accept a flow which is uniform in y at $x = 0$. These flows die out algebraically faster than that associated with λ_0 as $x \to \infty$ so the latter represents the asymptotic form of the flow as $x \to \infty$. As an eigenfunction it is multiplied by a coefficient which is determined by the matching (15*b*) in the present scheme. Equations (2) and (14*b*) can also be used to determine this coefficient and give the same value to eight significant figures. The $O(E^{-\frac{1}{3}})$ velocities associated with λ_0 can be rescaled into profile functions which are independent of x and c and depend only on α, $Y = yf^{-1}$ and $Z = -\zeta f^{-\frac{1}{3}}$, namely

$$u^c_{-\frac{1}{3}} = cf^{-\frac{4}{3}}U, \quad v^c_{-\frac{1}{3}} = cf^{-\frac{4}{3}}V.$$

Figure 4 gives profiles of U at the plane of symmetry $Y = 0$ for $\alpha = 0{\cdot}125$, 0·25 and 0·375, while figure 5 gives profiles of both U and V at $Y = 0$, 0·5 and 1·0 for $\alpha = 0{\cdot}25$.

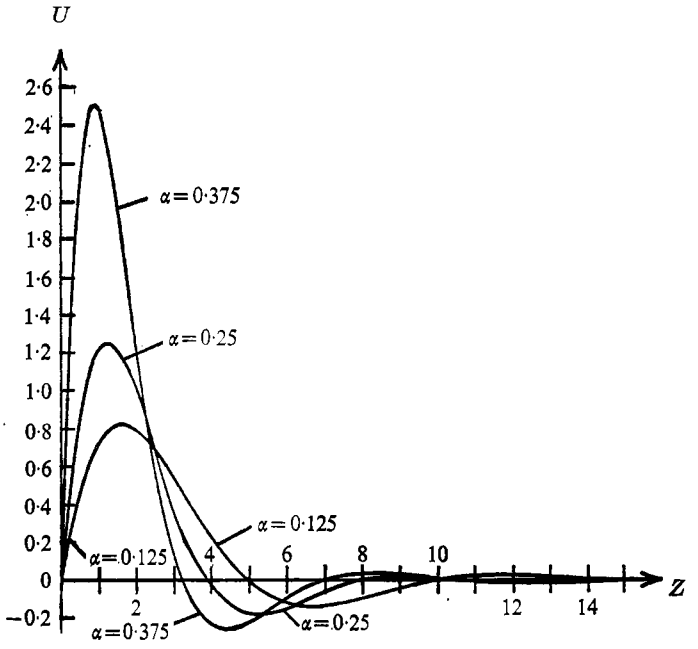

FIGURE 4. Profile function U at $Y = 0$ for $\alpha = 0{\cdot}125$, $0{\cdot}25$ and $0{\cdot}375$.

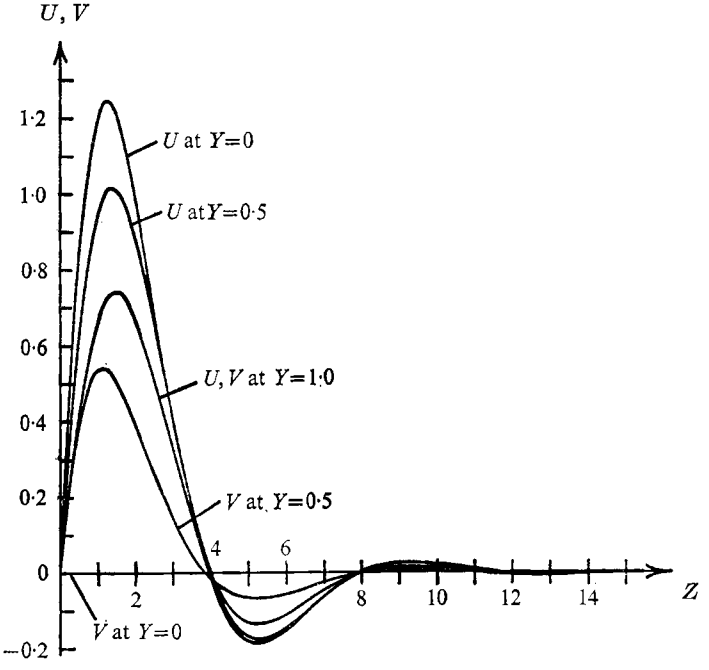

FIGURE 5. Profile functions U and V at $Y = 0$, $0{\cdot}5$ and $1{\cdot}0$ for $\alpha = 0{\cdot}25$.

For $\alpha = 0{\cdot}25$ the flow is forward ($U > 0$) and away from the plane of symmetry $Y = 0$ ($V > 0$) for $0 < Z < 4$ and for $8 < Z < 12$, but is backward ($U < 0$) and towards $Y = 0$ ($V < 0$) for $4 < Z < 8$ and for $12 < Z$. Both U and V are effectively zero beyond $Z = 15$. The velocity U at $Y = 0$ is slightly less than twice the value of U at $Y = 1$ for all Z. As α increases, the maximum value of U at $Y = 0$ increases while the Z values for $U = 0$ decrease, producing steeper velocity profiles. Also the ratio of U at $Y = 0$ to U at $Y = 1$ increases, so that the flow becomes more concentrated near the plane of symmetry $Y = 0$. As $\alpha \to 0$ the magnitude of U decreases while the Z values for which U remains appreciable increase. Physically, the side-layer thickness grows while the side-layer velocity decreases until the two side layers merge and become the core and $E^{\frac{1}{4}}$ and $E^{\frac{1}{3}}$ side layers for fully developed flow. Analytically, several intermediate analyses for small α would be needed to show how a flow carried by a high-velocity sheet jet adjacent to the side $z = 1$ evolves into the radically different fully developed flow.

5. Free shear layers at $x = 0$

The $E^{\frac{1}{4}}$ free shear layers (j) and (k) receive the total flow of $4c$ from the upstream core (d) and deliver it to the intersection regions (s) and (u), which pass it on to the downstream side layer (c). The variables in the upstream layer (j) are

$$u_0^j = \partial\Phi_0^j/\partial z, \quad v_0^j = -y\,\partial^4\Phi_0^j/\partial X^4, \quad w_{-\frac{1}{4}}^j = -\partial\Phi_0^j/\partial X, \tag{26}$$

where $\Phi_0^j(X, z)$ satisfies

$$2^{\frac{1}{2}}c\,\partial^4\Phi_0^j/\partial X^4 - \partial^2\Phi_0^j/\partial X^2 = 0. \tag{27}$$

Equation (27) follows from the $O(1)$ Ekman conditions at $y = \pm c$ and X is defined by (17 a). The solution of (27) which matches the upstream core solution is

$$\Phi_0^j = \Phi_0^d(0, z) + F_1(z)\exp(2^{-\frac{1}{4}}c^{-\frac{1}{2}}X),$$

where both $\Phi_0^d(0, z)$ and F_1 must be determined by matching the solution for the $E^{\frac{1}{3}}$ free shear layer.

The variables in the downstream $E^{\frac{1}{4}}$ shear layer (k) are given by (26) with j replaced by k, where $\Phi_0^k(X, z)$ satisfies

$$c\,\partial^4\Phi_0^k/\partial X^4 - 2^{-\frac{1}{2}}(1+s^2)^{\frac{1}{4}}\,\partial^2\Phi_0^k/\partial X^2 + s\,\partial\Phi_0^k/\partial z = 0, \tag{28}$$

which again follows from the $O(1)$ Ekman conditions at $y = \pm c$. Matching the downstream core and intersection region (p) gives the conditions

$$\Phi_0^p = -1 \quad \text{as} \quad X \to \infty \quad \text{and at} \quad z = -1. \tag{29a, b}$$

The Fourier cosine transform satisfying condition (29 a),

$$\Phi_0^k = -1 + 2\pi^{-1}\int_0^\infty \cos(tX)\,\overline{\phi}(t, z)\,dt,$$

reduces (28) to an ordinary differential equation in z with a solution

$$\overline{\phi} = b^{-1}\int_{-1}^{z} \{cF_2(z^*) - [ct^2 + 2^{-\frac{1}{2}}(1+s^2)^{\frac{1}{4}}]\,F_3(z^*)\} \times \exp\{-t^2b^{-1}[ct^2 + 2^{-\frac{1}{2}}(1+s^2)^{\frac{1}{4}}](z - z^*)\}\,dz^*,$$

which satisfies condition (29*b*). Here $F_2 = \partial\Phi_0^k/\partial X(0,z)$ and $F_3 = \partial^3\Phi_0^k/\partial X^3(0,z)$ are unknown functions of z.

Although the tangential velocities $u^j_{-\frac{1}{4}}$ and $\hat{v}^k_{-\frac{1}{4}} \doteq (1+s^2)^{-\frac{1}{2}}(u^k_{-\frac{1}{4}} \pm sv^k_{-\frac{1}{4}})$ in planes $z =$ constant are zero at $y = \pm c$, the corresponding tangential velocities $u^{j'}_{-\frac{1}{4}}$ and $\hat{v}^{k'}_{-\frac{1}{4}}$ in the Ekman layers above and below the $E^{\frac{1}{4}}$ free shear layers (j) and (k) are not zero, and at $X = 0$ these velocities account for an $O(E^{\frac{1}{4}})$ flow into or out of the Ekman layers (i') above and below the $E^{\frac{1}{4}}$ free shear layer (i). The flow into (or out of) these Ekman layers (i') from the upstream Ekman layers (j') is not equal to the flow into (or out of) the downstream layers (k') and the difference appears as a line source (or sink) at $\eta = 0$, $y = c$ and an equal line sink (or source) at $\eta = 0$, $y = -c$, where η is defined by (17*b*). The source and sink drive the flow in the $E^{\frac{1}{4}}$ free shear layer (i) (Howard 1969). This flow involves the variables $u^i_{\frac{1}{4}}$, $v^i_{-\frac{1}{12}}$, $w^i_{-\frac{1}{12}}$ and $\Phi^i_{\frac{1}{4}}$ while

$$\Phi_0^i = \Phi_0^j(0,z), \quad \Phi^i_{\frac{1}{12}} = \Phi^j_{\frac{1}{12}}(0,z) + \eta\,\partial\Phi_0^j/\partial X(0,z),$$

$$\Phi^i_{\frac{1}{6}} = \Phi^j_{\frac{1}{6}}(0,z) + \eta\,\partial\Phi^j_{\frac{1}{12}}/\partial X(0,z) + \tfrac{1}{2}\eta^2\,\partial^2\Phi_0^j/\partial X^2(0,z).$$

Therefore
$$\Phi_0^j(0,z) = \Phi_0^k(0,z), \quad \partial\Phi_0^j/\partial X(0,z) = \partial\Phi_0^k/\partial X(0,z), \tag{30a,b}$$

$$\partial^2\Phi_0^j/\partial X^2(0,z) = \partial^2\Phi_0^k/\partial X^2(0,z), \tag{30c}$$

$$\partial^3\Phi_0^j/\partial X^3(0,z) = \partial^3\Phi_0^k/\partial X^3(0,z) + F_4(z), \tag{30d}$$

where F_4 is related to the strength of the source and sink at $\eta = 0$, $y = \pm c$, which in turn is related to F_1, F_2 and F_3.

The unknown functions $\Phi_0^d(0,z)$, F_1, F_2 and F_3 are now determined by conditions (30). Condition (30*b*) gives

$$F_2 = 2^{-\frac{1}{4}}c^{-\frac{1}{2}}F_1$$

and condition (30*d*) gives

$$F_3 = 2^{-\frac{3}{4}}c^{-\frac{3}{2}}F_1 - F_4.$$

Condition (30*c*) now gives a Volterra integral equation governing F_1. This equation has the form of a Laplace convolution with a kernel given by a Fourier cosine inversion. Once this equation is solved condition (30*a*) gives $\Phi_0^d(0,z)$, so that the boundary-value problem governing $\Phi_0^d(x,z)$ is complete. In this scheme the Volterra equation is homogeneous and its solution can be multiplied by an arbitrary constant. This constant is determined by the condition

$$\Phi_0^d(0,1) = 1,$$

which is equivalent to the normalization (2).

This analysis for the free shear layers has not actually been carried out since the object of the present paper is to obtain solutions for the high-velocity side layers in both the constant-area and variable-area ducts and these solutions do not depend on the solutions for the free shear layers or for the upstream core. Although specific solutions for the upstream core for various α have not been obtained, a simple separation-of-variables argument indicates that the most persistent part of the disturbance to the upstream fully developed flow dies out like $\exp(\frac{1}{2}\pi x)$ for all α.

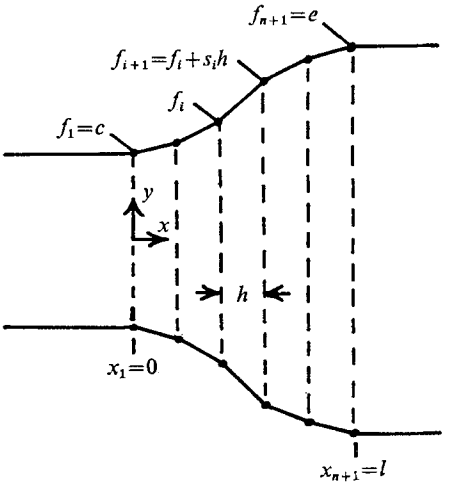

FIGURE 6. z section used to approximate a general diverging duct between two constant-area ducts.

6. General duct geometries

The analysis presented in §§3 and 4 for a prototype with straight walls can be extended to more general rectangular ducts with parallel sides. For a general diverging duct placed between two constant-area ducts with

$$f = \begin{cases} c & \text{for} \quad x < 0, \\ e & \text{for} \quad x > l, \end{cases}$$

the top and bottom of the diverging duct are approximated by series of straight walls connecting the lines

$$x_i = (i-1)h, \quad y_i = \pm f_i = \pm f(x_i) \quad (i = 1, 2, 3, \ldots, n+1),$$

where $l = nh$, as shown in figure 6. For the ith segment ($x_i < x < x_{i+1}$) the side-layer eigenvalue problems derived in §3 are solved for

$$\alpha_i = \pi^{-1} \arctan [h^{-1}(f_{i+1} - f_i)].$$

The solutions for the core and $E^{\frac{1}{3}}$ side layers at $z = \pm 1$ in this segment are expanded in the eigenfunctions corresponding to all the eigenvalues $\lambda_j^{(i)}$ and $\gamma_j^{(i)}$ for this α_i. In the upstream constant-area duct ($x < 0$) there is a high-velocity $E^{\frac{1}{3}}$ side layer at $z = -1$ which carries no net flow (see figure 7) and which involves a set of unknown coefficients A_m ($m = 1, 2, 3, \ldots$), while $\Phi_0 = 1$ and $\mathbf{v}_{-\frac{1}{3}} = 0$ throughout the $E^{\frac{1}{3}}$ side layer at $z = 1$. In the downstream constant-area duct ($x > l$) $\Phi_0 =$ constant and $\mathbf{v}_{-\frac{1}{3}} = 0$ throughout the $E^{\frac{1}{3}}$ side layer at $z = -1$, while there is a high-velocity $E^{\frac{1}{3}}$ layer at $z = 1$ which also carries no net flow and which involves another set of unknown coefficients C_m ($m = 1, 2, 3, \ldots$), where

$$c_m = C_m \exp [m\pi e^{-1}(l-x)]$$

are the functions of x in the series (22) which satisfy (23d) with $c = e$. The unknown coefficients in the n eigenfunction expansions for the solutions in the

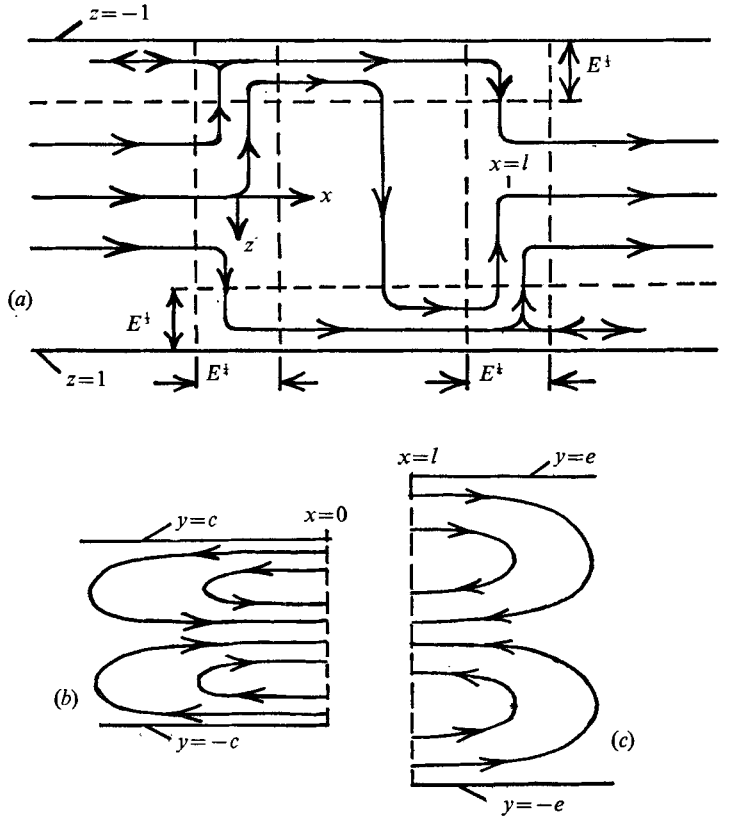

FIGURE 7. Sketch of streamlines for a general expansion placed between two constant-area ducts. (*a*) x, z plane. (*b*) Upstream $E^{\frac{1}{3}}$ side layer at $z = -1$. (*c*) Downstream $E^{\frac{1}{3}}$ side layer at $z = 1$.

n segments of the diverging duct as well as A_m and C_m are determined by applying the matching (15) at each join between segments: $x = x_i$ for $i = 1, 2, \ldots, n+1$. There is an $E^{\frac{1}{3}}$ free shear layer between two $E^{\frac{1}{4}}$ free shear layers at each join x_i and there is an $O(1)$ flow across the duct within each pair of $E^{\frac{1}{4}}$ layers. These layers obviously do not occur in the original duct with smooth top and bottom. In a qualitative way the transverse core flow in the original duct is divided in the approximate duct into a flow associated with the local wall slope, which is still carried by the core, and a flow associated with the wall curvature, which is now concentrated in the free shear layers. The limiting process $h \to 0$ and $n \to \infty$ is not a simple one. As h is reduced from $O(1)$ to $O(E^{\frac{1}{4}})$, $\alpha_{i+1} - \alpha_i$ diminishes from $O(1)$ to $O(E^{\frac{1}{4}})$ and the transverse velocity in the $E^{\frac{1}{4}}$ free shear layers diminishes from $O(E^{-\frac{1}{4}})$ to $O(1)$, while the $E^{\frac{1}{4}}$ layers at adjacent joins merge and become the core. Thus the core flow in the approximate duct is quite different from that in the original duct and the evolution of the former into the latter would require a special analysis for $h = O(E^{\frac{1}{4}})$ and perhaps another for $h = O(E^{\frac{1}{3}})$, i.e. when the $E^{\frac{1}{3}}$ free shear layers merge. However the side-layer solutions for the approximate duct are good approximations to those for the original duct and it is these high-

velocity sheet jets which carry the flow along the duct. If an even better approximation of the side-layer solutions is required, the present approximate solutions could be used as initial values in a numerical relaxation solution of the basic equations derived from (5 *c*, *d*), (7 *c*), (10) and (11).

The extension to ducts with symmetrically diverging or converging sides at $z = \pm g(x)$ is relatively simple. Physically, the harmonic flow in duct segments with parallel top and bottom adjusts to the boundary conditions being applied at $z = \pm g$ instead of at $z = \pm 1$ and the high-velocity side layers in segments with diverging or converging top and bottom simply follow the sides with no change of structure. This extension is discussed in more detail by Walker, Ludford & Hunt (1972) for the analogous problem of MHD flow in variable-area rectangular ducts with strong magnetic fields applied in the y direction.

The present analysis coupled with that for variable-area circular ducts (Walker 1974) can be extended to the flow in rapidly rotating ducts with any cross-sections which diverge or converge symmetrically about a centre-line which is perpendicular to the axis of rotation.

The author is deeply indebted to Dr J. C. R. Hunt and Dr G. S. S. Ludford for arousing his interest in the present problem. This research was supported by the National Science Foundation under Grant GK 37427.

REFERENCES

BARCILON, V. 1967 On the motion due to sources and sinks distributed along the vertical boundary of a rotating fluid. *J. Fluid Mech.* **27**, 551–560.

GREENSPAN, H. P. 1968 *The Theory of Rotating Fluids*. Cambridge University Press.

HOWARD, L. N. 1969 *Rotating Flow*. Lectures at the Royal Institute of Technology, Stockholm.

WALKER, J. S. 1974 Steady flow in rapidly rotating circular expansions. *J. Fluid Mech.* **66**, 657–671.

WALKER, J. S., LUDFORD, G. S. S. & HUNT, J. C. R. 1972 Three-dimensional MHD duct flows with strong transverse magnetic fields. Part 3. Variable-area rectangular ducts with insulating walls. *J. Fluid Mech.* **56**, 121–141.